Journal of Glaciology, Vol. 12, No. 66, 1973

THE EFFECT OF CONFINING PRESSURE ON THE MECHANICAL PROPERTIES OF SAND–ICE MATERIALS

By Bernard D. Alkire

(Department of Civil Engineering, Michigan Technological University, Houghton, Michigan 49931, U.S.A.)

and Orlando B. Andersland

(Department of Civil Engineering, Michigan State University, East Lansing, Michigan 48823, U.S.A.)

Abstract. Cylindrical samples containing 0.59 mm to 0.84 mm diameter silica sand at about 97% and 55% ice saturation (the ratio of ice volume to sand pore volume) were tested at a temperature of −12° C in triaxial compression. Both constant axial strain-rate tests and step-stress creep tests provide information on the influence of confining pressure on the shear strength and creep behavior of the sand–ice material. Changes in the degree of ice saturation help show the influence of the ice matrix versus the sand material on the mechanical behavior. Data are discussed in terms of the Mohr–Coulomb failure law and creep theories. It is shown that the cohesive component of strength depends on response of the ice matrix, whereas the frictional component of strength responds in a manner very similar to unfrozen sand tested at high confining pressures. Experimental data show that creep rates decrease exponentially and creep strength increases with an increase in confining pressure.

Résumé. *Les effets de la pression ambiante sur les propriétés mécaniques du mélange sol–glace.* Des échantillons cylindriques contenant un sable siliceux de 0,59 à 0,84 mm de diamètre a environ 97% et 55% de saturation en glace, ont été essayés à une température de 12° C en compression triaxiale. Les essais à vitesse de déformation axiale constante comme ceux montrant le fluage sous contrainte croissante procurent des informations sur l'influence de la pression ambiante sur la résistance au cisaillement et sur le comportement au fluage du mélange sable–glace. Les changements dans le degré de saturation en glace montreront, espère-t-on, les influences respectives de la matrice de glace et du matériel sableux dans le comportement mécanique. Les résultats sont discutés à partir de la loi de rupture de Mohr-Coulomb et des théories du fluage. On montre que la composante de cohésion de la résistance dépend de la réponse de la matrice de glace, tandis que la composante de friction de cette résistance répond de manière très analogue à celle d'un sable non gelé sous fortes pressions. Les données expérimentales montrent que les vitesses de fluage décroissent exponentiellement, et la résistance au fluage croît lorsque s'accroît la pression ambiante.

Zusammenfassung. *Die Wirkung allseitigen Druckes auf die mechanischen Eigenschaften eines Sand-Eis-Gemisches.* Zylindrische Proben von Si-Sanden mit Korngrössen von 0,59 mm–0,84 mm und Eissättigungen von ungefähr 97% und 55% wurden bei einer Temperatur von −12° C unter dreiachsigem Druck untersucht. Sowohl die Versuche mit konstanter axialer Belastung als auch die Kriechtests mit schrittweiser Spannungsänderung liefern Informationen über den Einfluss des allseitigen Druckes auf den Scherwiderstand und das Kriechverhalten des Sand-Eis-Gemisches. Mit Hilfe von Veränderungen des Grades der Eissättigung kann der Einfluss der Eismatrix gegenüber dem sandigen Material auf das mechanische Verhalten gezeigt werden. Die Ergebnisse werden aus der Sicht des Mohr-Coulomb'schen Bruchgesetzes und der Theorien des Kriechens diskutiert. Es wird nachgewiesen, dass die Kohäsionskomponente der Festigkeit von der Reaktion der Eismatrix abhängt, während die Reibungskomponente der Festigkeit sich sehr ähnlich wie bei nichtgefrorenem Sand verhält, der hohen allseitigen Drücken ausgesetzt ist. Die Versuchsergebnisse zeigen, dass mit anwachsendem allseitigen Druck die Kriechgeschwindigkeit exponentiell abnimmt und die Kriechfestigkeit zunimmt.

Symbols

b	intercept of the axial strain-rate versus deviator stress curves.
c	cohesion.
C_i	intercept of the ith segment of the m versus confining pressure curve.
D	$\sigma_1-\sigma_3$ = axial stress difference = deviator stress.
D_H	applied deviator stress for high ice content.
D_L	applied deviator stress for low ice content.
G_i	slope of the ith segment of the m versus confining pressure curve.
$\mathcal{J}$	degree of ice saturation.
m	slope of axial strain-rate versus deviator stress curves.
p	$(\sigma_1+\sigma_3)/2$.

q $(\sigma_1-\sigma_3)/2$.
α slope of q_f versus p_f curve.
$\dot{\epsilon}_1$ axial creep rate.
ϕ angle of internal friction.
σ_1 major principal stress.
σ_2 intermediate principal stress.
σ_3 minor principal stress = confining pressure.
σ_m mean normal stress = $\frac{1}{3}(\sigma_1+\sigma_2+\sigma_3)$.
σ_{ff} normal stress on failure plane at failure.
τ_{ff} shear stress on failure surface at failure.

Introduction

Confining pressure alters the mechanical behavior of sand–ice materials primarily by its influence on sliding friction, particle re-orientation, and reduction in dilatancy effect. Particle crushing under high pressures serves to increase sand density with a corresponding increase in shear strength. For low sand contents and particles not in contact, the frozen soil behavior is dependent on the properties of the ice matrix (Goughnour and Andersland, 1968). Confining pressures limit or reduce crack and cavity formation and alter accommodation cracking and distortion along grain boundaries within the ice. With confining pressures greater than 62 MN/m^2 and ice saturated sand materials, pressure melting and ice/water phase changes are responsible for a decrease in shear strength (Chamberlain and others, 1972). Increased pore pressures and no drainage reduce effective intergranular contacts thereby reducing sliding friction. Other factors responsible for altering the mechanical behavior include strain-rate, temperature, stress history, and the presence of impurities such as air bubbles, salts, or organic matter in the ice matrix (Scott, 1969; Tsytovich, 1959, p. 108–52).

To provide additional information on the influence of confining pressure on the shear strength and creep behavior of sand–ice materials, a series of constant axial strain-rate tests and uniaxial, confined and step-stress creep tests were performed using triaxial apparatus (Alkire, unpublished).

Test materials and sample preparation

A pure silica (Ottawa) sand with particle diameters from 0.59 mm to 0.84 mm was used for all sand–ice test samples. Sand–ice samples, 2.87 cm in diameter by 5.74 cm high, were prepared by pouring sand into an aluminum mold and vibrating until the predetermined amount of sand was level with the top of the mold. Precooled, distilled, de-ionized, and de-aired water was next poured into the sand and frozen at a temperature close to $-18°$ C. A few sand particles were lost dependent on the amount of trimming needed to permit uniform seating of the loading cap. Hence void ratios computed on the basis of trimmed sample volume, oven dry weight of sand, and specific gravity of the sand did show a small scatter. Since vacuum saturation was not used, a few air bubbles trapped in the sand lowered the degree of ice saturation to about 97%. An intermediate degree of ice saturation, close to 55%, gave approximately equal amounts of ice (less than 4% difference) in the upper and lower halves of the frozen sand–ice sample when prepared in a similar manner. After a 24 h freezing period the samples were trimmed, removed from the mold, and weighed in air and kerosene. Density of the polycrystalline ice within the sand pores ranged from 0.854 Mg/m^3 to 0.918 Mg/m^3. Friction reducers were placed at each end of the sample prior to mounting in a precooled high-pressure triaxial cell. Three or more thin rubber membranes protected the sample from the coolant liquid. Immediate placement in a cold bath and storage for 12 h before testing permitted temperature equalization throughout the sample and cell.

Equipment and test procedures

The triaxial cell was immersed in a coolant mixture of ethylene glycol and water maintained at a constant temperature of -12° C by coolant circulation through an adjacent portable refrigerated bath. Sample temperatures during a test varied by no more than ± 0.05 deg. Axial loads were measured by means of a force transducer mounted in the base of the triaxial cell, thereby avoiding ram friction in load observations. Axial deformations, determined by means of a linear differential transformer, were recorded with an accuracy better than $\pm 10^{-3}$ cm. Confining pressures up to 7 MN/m^2 were applied to test samples via pressurized nitrogen acting on the coolant liquid in the triaxial cell. Constant axial deformation rates were applied to the loading ram of the triaxial cell by means of a variable-speed mechanical loading system. Axial loads for creep tests were applied to the ram and sample by means of a load frame supporting a dead load of lead bricks. Confining pressure was removed or added to produce step changes in deviator stress. During sample deformation, a constant unit stress was maintained by adding lead shot to the dead weights to compensate for the small increase in sample area. Constant sample volume was assumed for this correction.

Experimental results

Constant axial strain-rate tests

Typical stress–strain curves for sand–ice samples deformed at 0.002 66 min^{-1} are shown in Figure 1. For convenience and clarity, only selected data points are shown. These were based on a continuous record obtained using load and displacement transducers (Alkire, unpublished). For the higher confining pressures, the curves show an initial yield followed by a second, approximately linear, portion leading to failure at a larger deviator stress. The first yield occurs at around 0.01 axial strain which is close to that observed for yield of polycrystalline ice (Goughnour and Andersland, 1968). The peak stress occurs at larger strains

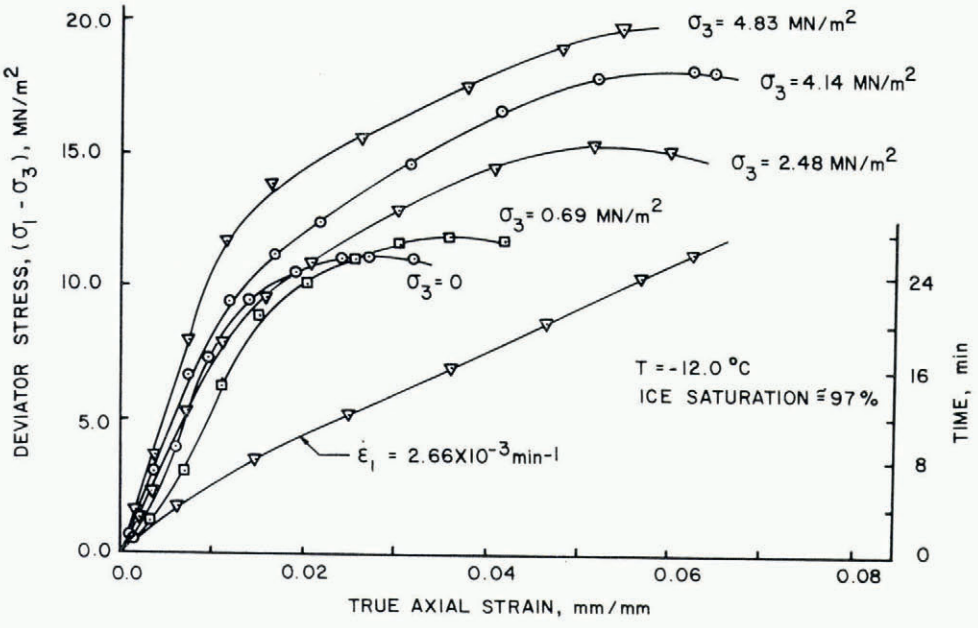

Fig. 1. Influence of confining pressure on the stress–strain behavior of sand–ice material at 97% ice saturation.

https://doi.org/10.3189/S0022143000031889 Published online by Cambridge University Press

and appears to be related to the increase in frictional resistance. This behavior has also been observed for unfrozen clay soils in which the cohesion component of strength develops to its maximum value at small axial compression strains, while the frictional component of strength requires larger strains to fully develop (Schmertmann and Osterberg [1961]).

It is essential that samples with similar void ratio be used in making the above comparisons. Stress–strain curves for three sand–ice samples with slightly different initial void ratios are shown in Figure 2. For the same confining pressure, 4.826 MN/m², a change in void ratio of less than 0.03 results in a significant change in the stress–strain curve.

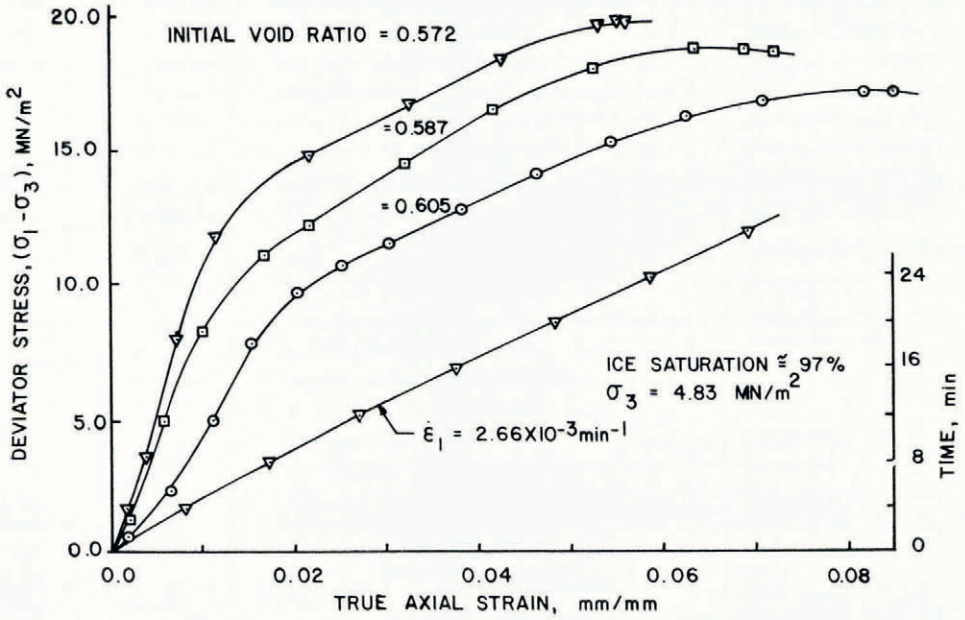

Fig. 2. Influence of void ratio on the stress–strain behavior.

The influence of reduced ice content on stress–strain curves is shown in Figure 3 for the same axial strain-rate and temperature. For an ice saturation of 55%, the initial yield followed by a second linear portion again develops at higher confining pressures. The peak deviator stress has been reduced in comparison to the curves on Figure 1 with similar confining pressures. This is an indication of the reduced load-carrying capacity for samples with smaller amounts of ice in the void spaces.

Creep tests

Step-stress creep data shown in Figure 4 include three levels of deviator stress $D = (\sigma_1 - \sigma_3)$, and seven levels of confining pressure σ_3. Minimum creep rates and the percent of maximum deviator stress are given for each section of the curve. The jump in strain at each increase in confining pressure corresponds to cell expansion as recorded by the displacement transducer. Step-stress creep data shown in Figure 5 include two levels of deviator stress and seven levels of confining pressure for an ice saturation of 60%. For the same deviator stress, comparison with Figure 4 shows a much larger creep strain with the reduced ice content. The per cent of maximum deviator stress shown on Figures 4 and 5 refer to the maximum shear strength based on the constant axial strain-rate tests.

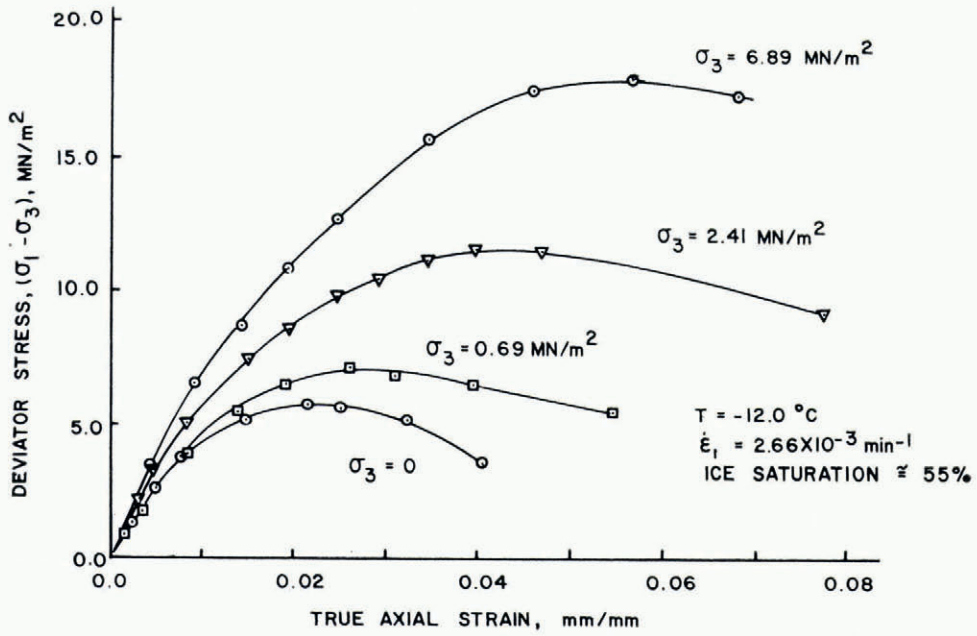

Fig. 3. Influence of confining pressure on the stress–strain behavior of a sand–ice material at 55% ice saturation.

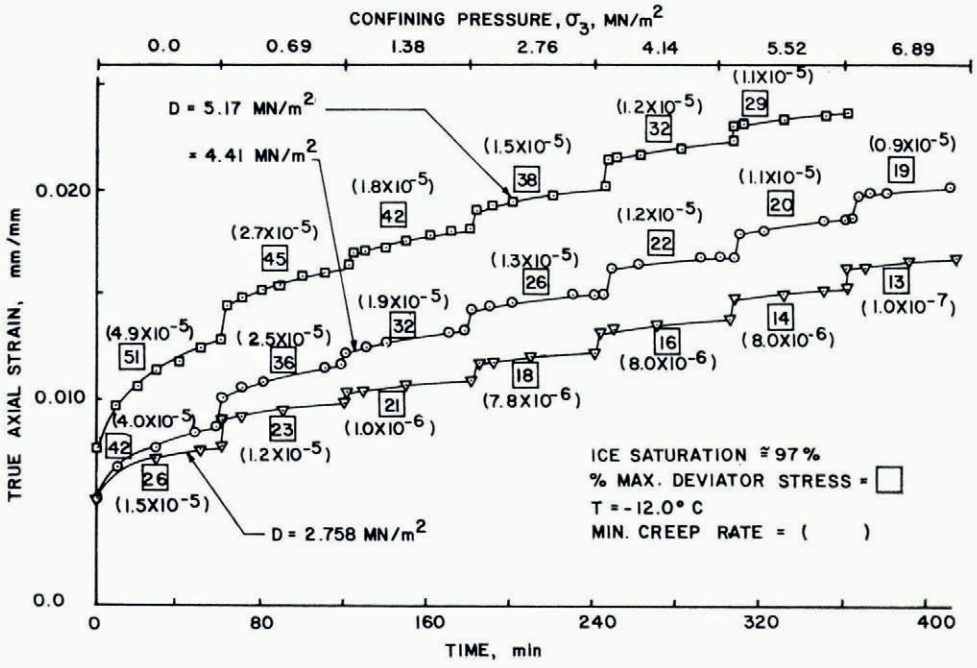

Fig. 4. Step-stress creep curves for high ice saturation sand–ice samples and constant deviator stresses.

https://doi.org/10.3189/S0022143000031889 Published online by Cambridge University Press

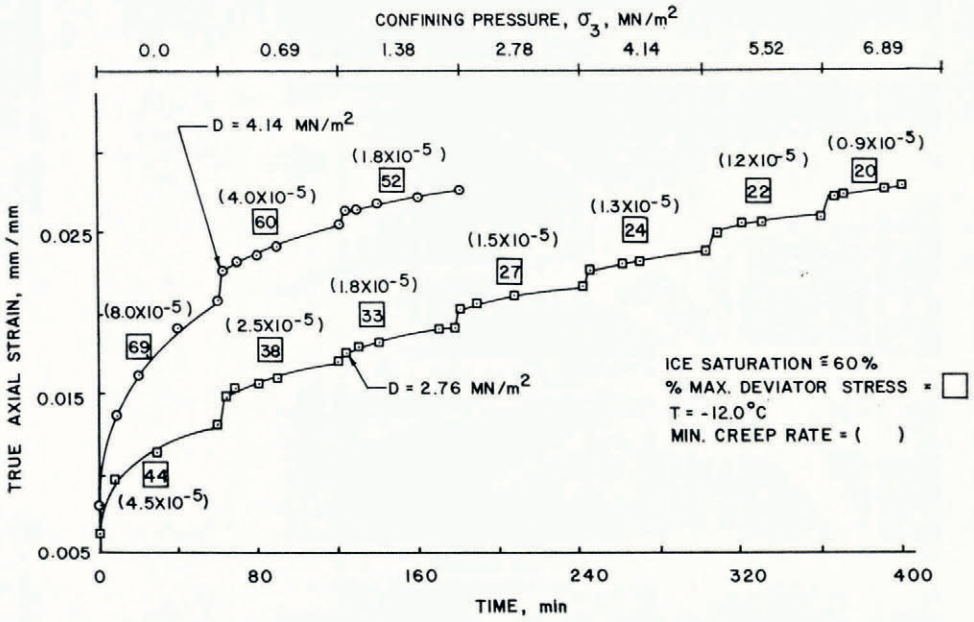

Fig. 5. Step-stress creep curves for low ice saturated sand–ice samples and constant deviator stresses.

Interpretation of results

To interpret the experimental results, several factors need to be discussed. They include confining pressure, void ratio, reduced ice content, failure criteria, and creep behavior.

Confining pressure

Constant axial strain-rate tests summarized in Figure 1 show that confining pressure has a substantial strengthening effect on the sand–ice samples. The curves show that the cohesive component of strength due to the ice matrix develops to its maximum value at axial compression strains close to 0.01, while the frictional component of strength continues to develop to its maximum value at a much larger axial strain. Failure strains up to 0.06 correspond to the higher confining pressures. As the confining pressure is increased the material appears to become increasingly dependent on the frictional nature of the sand. This fact is more clearly shown in Figure 6 where the maximum principal stress ratio has been plotted against confining pressure. Comparisons with data for unfrozen silica sand shows that the cohesive component becomes very small when confining pressures approached 7 MN/m^2. For the low ranges of confining pressure, the behavior of sand–ice material depends primarily on the cohesive nature of the ice matrix.

Void ratio

The large influence which small changes in initial void ratio have on the stress–strain behavior of sand–ice material is shown in Figure 2. For a constant confining pressure of 4.826 MN/m^2 the sliding friction and particle reorientation effect should be relatively constant. Particle crushing is negligible for silica sand for the range of confining pressures used in this study (Lee and Seed, 1967). Therefore, the dilatancy component would appear to be primarily responsible for the change in the stress–strain curves. For unfrozen sand dilatancy increases the shear strength by requiring energy to move particles up and over one another.

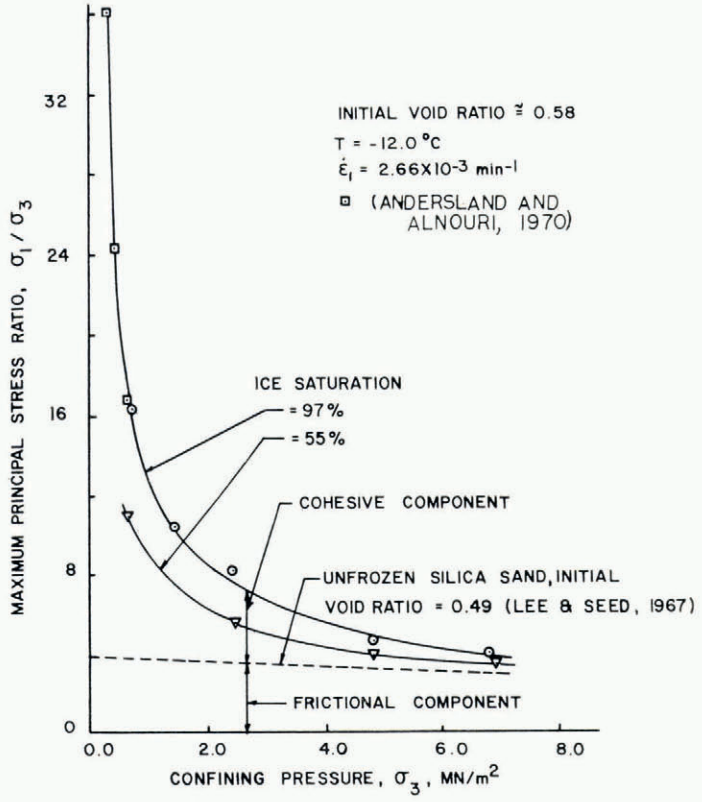

Fig. 6. Maximum principal stress ratio at failure versus confining pressure for frozen and unfrozen silica sand.

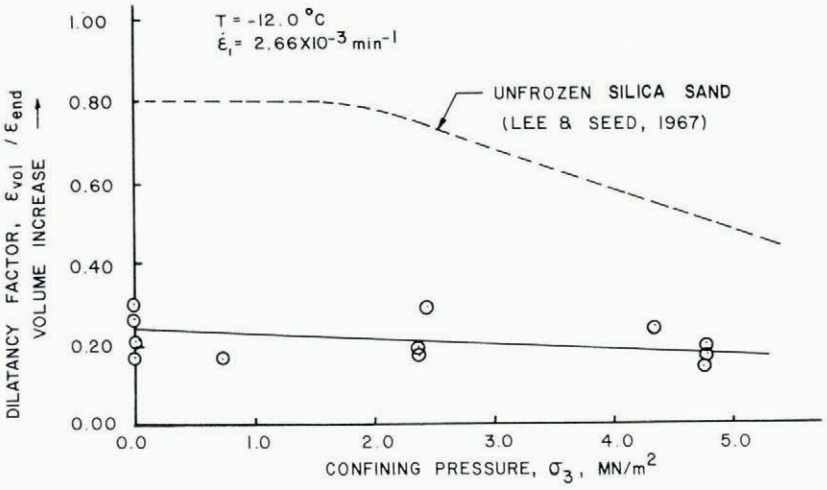

Fig. 7. Confining pressure versus volume change for the triaxial compression tests.

https://doi.org/10.3189/S0022143000031889 Published online by Cambridge University Press

For a sand–ice material energy is required to overcome the forces of adhesion between the ice and sand, hence it would be expected that the increase in deviator stress for a small change in void ratio would be greater than for unfrozen sand. Equipment limitations did not permit measurement of volume changes during the triaxial tests, however volume measurements taken before and after each test, given in Figure 7, show a volume increase for all samples tested at the lower confining pressures. Data from Lee and Seed (1967) given in Figure 7 for unfrozen silica sand show that the dilatancy factor is suppressed with increased confining pressure. A similar trend is noted for the sand–ice material.

Reduced ice content

A comparison of stress–strain curves in Figures 1 and 3 show a reduced deviator stress for sand–ice samples with an ice saturation of 55%. A summary of these data shown in Figure 8 suggests that the reduction in deviator stress is in proportion to the amount of ice in the sand voids. Only two levels of ice saturation are included because of difficulty in obtaining a

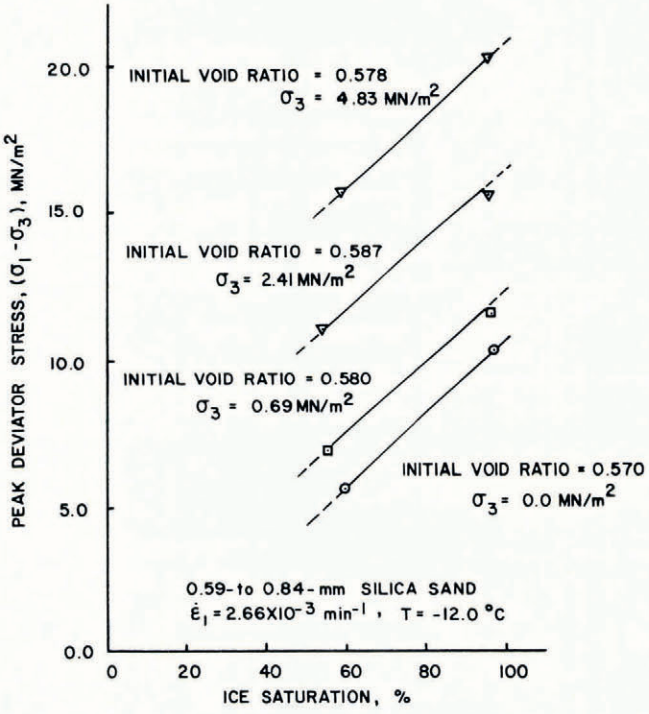

Fig. 8. Peak deviator stress versus ice saturation for various confining pressures.

uniform ice distribution within the samples at other ice contents. For the four levels of confining pressure and small differences in void ratio, the parallel lines indicate that the reduction in peak deviator stress is due primarily to a decrease in cohesion of the ice matrix. A similar relationship has been reported by Kaplar (1971) and Vyalov (1959). A linear extrapolation of the lower curve to zero deviator stress suggests that about 18% ice saturation is required to develop any significant strength for zero confining pressure. The curves do not extend beyond 100% ice saturation.

Failure criteria

Constant strain-rate data are summarized in Figure 9 in terms of the maximum shear stress at failure. It was convenient to let

$$p = \tfrac{1}{2}(\sigma_1+\sigma_3) \tag{1a}$$

and

$$q = \tfrac{1}{2}(\sigma_1-\sigma_3) \tag{1b}$$

represent the coordinates of a stress point. The normal stresses, σ_1 and σ_3, represent the major and minor principal stresses at failure, respectively. A series of tests with different confining pressures define K_f-lines as shown in Figure 9 for silica sand at two levels of ice saturation.

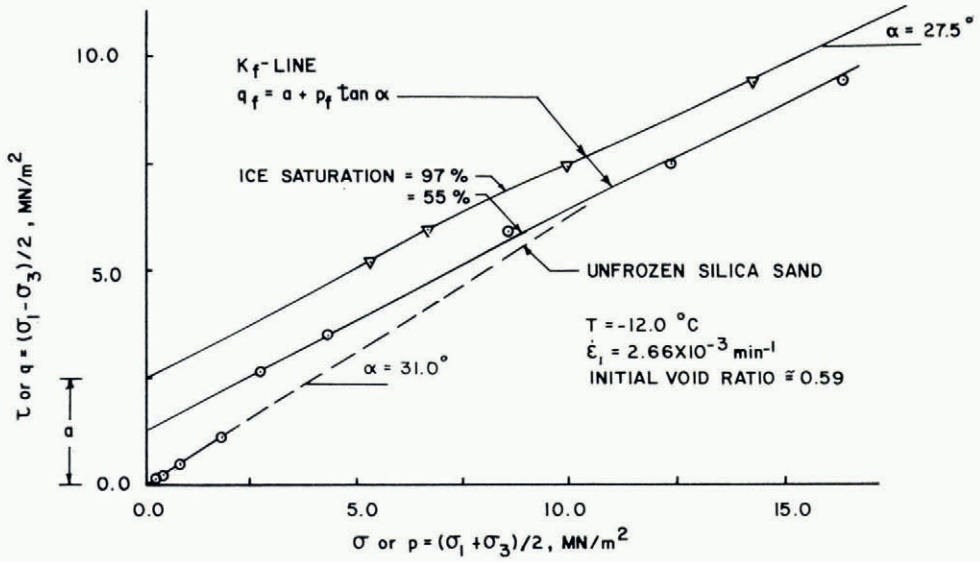

Fig. 9. K_f failure lines for frozen and unfrozen silica sand based on constant axial strain-rate triaxial tests.

The slope angle α appears to be reasonably constant for the range of normal stresses considered and the intercept a is dependent on the degree of ice saturation. Geometric transformation gives

$$\phi = \sin^{-1}\tan\alpha \tag{2a}$$

and

$$c = a/\cos\phi \tag{2b}$$

where ϕ is the angle of internal friction and c the cohesion. Using the Mohr–Coulomb failure law (Lambe and Whitman, 1969; Wu, 1966) the shear strength of the sand–ice material will be

$$\tau_{ff} = c+\sigma_{ff}\tan\phi \tag{3}$$

where τ_{ff} is the shear stress on the failure surface at failure and σ_{ff} the normal stress on that plane at failure. The apparent angle of internal friction, ϕ, for the high ice saturation, equal to 31.4°, is less than the friction angle of 37° for the unfrozen sand (Alkire, unpublished). The ice interferes with full development of frictional resistance, perhaps by limiting effective intergranular contact between sand particles. Using the K_f-line for unfrozen sand as a basis for separating the frictional and cohesive components of shear strength, the data also suggest a decrease in the cohesion as confining pressures increase, in agreement with data shown in Figure 6.

https://doi.org/10.3189/S0022143000031889 Published online by Cambridge University Press

The above analysis, by necessity, must be based on total stresses. When the ice saturation approaches 100% the sand–ice behavior may be analogous to undrained tests on saturated soil where the slope angle α would decrease to zero. Evidence of this behavior has been given by Chamberlain and others (1972). Their data show a decrease in strength when confining pressure becomes large enough to induce pressure melting and ice/water phase changes in ice-saturated sand. The development of excess pore-water pressures reduces intergranular contacts, thereby reducing sliding friction.

Creep behavior

Step-stress creep tests were used by Andersland and AlNouri (1970) to show that a linear relationship exists between secondary creep rate and a term which included both deviator stress, $D = (\sigma_1 - \sigma_3)$, and mean stress, $\frac{1}{3}(\sigma_1 + \sigma_2 + \sigma_3)$. Using the same test techniques, the data shown in Figures 4 and 5 extend the range of confining pressures to 6.89 MN/m². The new data confirm earlier results for confining pressures up to about 1.38 MN/m². At higher pressures the observed strain-rates are greater than would be predicted on the basis of data taken at low confining pressures.

A plot of deviator stress versus axial strain-rate for each level of confining pressure, as shown in Figure 10, illustrates their inter-relationship. Time dependency has been eliminated by using the minimum strain-rates observed at the end of each hour during step loading. The

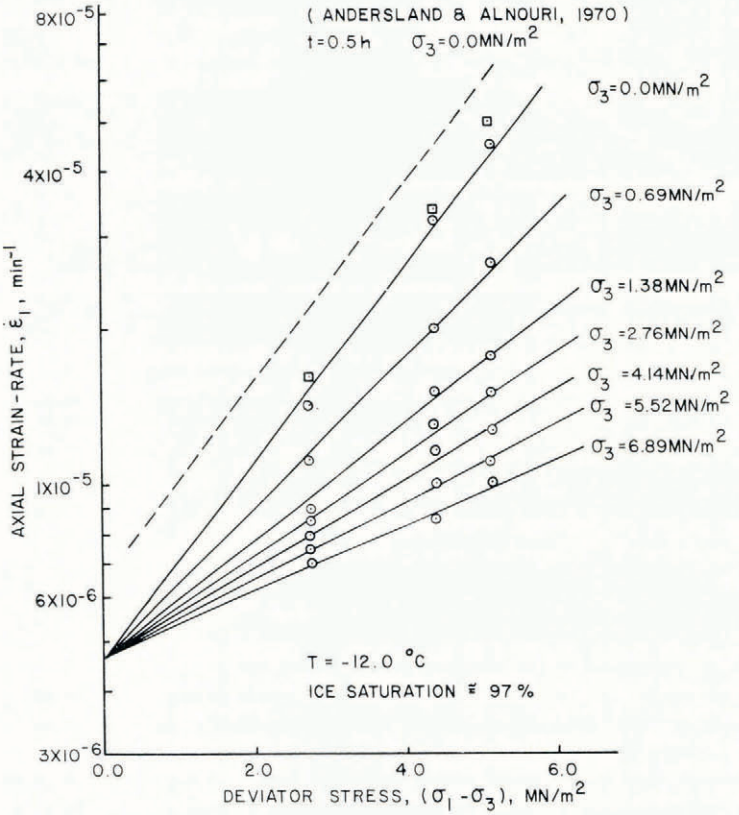

Fig. 10. Effect of confining pressure on axial strain-rates for sand–ice with high ice saturation. (Strain-rates obtained at 1 h intervals except as noted.)

https://doi.org/10.3189/S0022143000031889 Published online by Cambridge University Press

decrease in strain-rate with increase in confining pressure corresponds to the decrease in slope of the family of lines. The axial creep rate $\dot{\epsilon}_1$ may be expressed as

$$\dot{\epsilon}_1 = b(t) \exp mD. \tag{4}$$

Taking the logarithm of both sides of Equation (4) gives

$$\log \dot{\epsilon}_1 = \log b(t) + (0.4343m)D \tag{5}$$

where $(0.4343m)$ is the absolute value of the slope of the lines of equal confining pressure, D is the deviator stress equal to $(\sigma_1 - \sigma_3)$, and b is the time-dependent intercept on the ordinate.

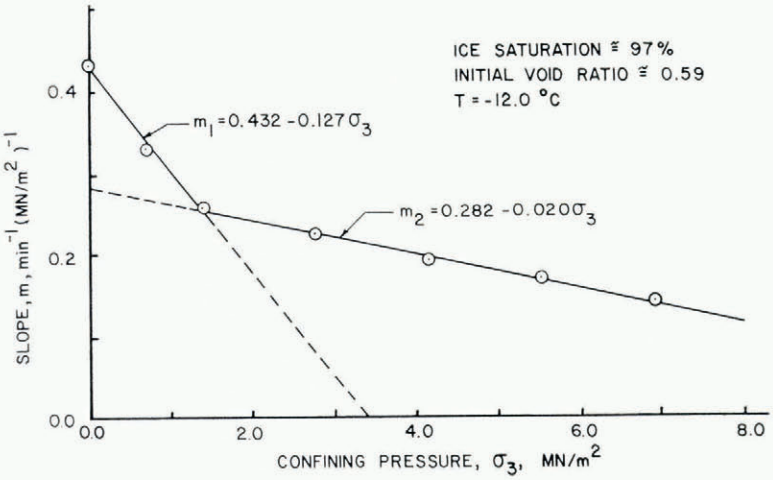

Fig. 11. Graphical determination of the coefficients used in Equation (4).

Values of m versus confining pressure plotted in Figure 11 give a bilinear relationship with the equation

$$m_i = C_i + G_i\sigma_3 \tag{6}$$

where C_i is the intercept and G_i the slope for the respective segment. The two lines intersect at a confining pressure of 1.38 MN/m². Combining Equations (4) and (6) gives

$$\dot{\epsilon}_1 = b(t) \exp (C_iD) \exp (G_i\sigma_3D) \tag{7}$$

where $b(t)$ equals 4.7×10^{-6} min^{-1} for time intervals equal to 60 min during step-stress loading. For $\sigma_3 \leqslant 1.38$ MN/m², C_1 equals 0.432 min^{-1} (MN/m²)$^{-1}$ and G_1 equals 0.127 min^{-1} (MN/m²)$^{-2}$; and for $\sigma_3 > 1.38$ MN/m², C_2 equals 0.282 min^{-1} (MN/m²)$^{-1}$ and G_2 equals 0.020 min^{-1} (MN/m²)$^{-2}$. Equation (7) shows that creep rates are more responsive to confining pressures below 1.38 MN/m². The term $b(t)$ presumably is related to the structural changes which occur in the sand–ice material during creep.

For the reduced ice content step-stress creep data shown in Figure 5, Equation (7) is also applicable. The deviator stress for the reduced ice content D_L is set equal to the deviator stress for the high ice content D_H times the degree of ice saturation $\mathcal{J}$ expressed as a decimal. Substitution into Equation (7) gives

$$\dot{\epsilon}_1 = b(t) \exp\left(\frac{C_iD_L}{\mathcal{J}}\right) \exp\left(\frac{G_i\sigma_3D_L}{\mathcal{J}}\right). \tag{8}$$

The parameters $b(t)$, C_i, and G_i for the low degree of ice saturation approximate the values based on the high degree of ice saturation. Calculated and experimental strain-rates were in excellent agreement (Alkire, unpublished).

Summary and conclusions

Constant strain-rate tests and step-stress creep tests show the effect of confining pressure on the mechanical behavior of sand–ice samples prepared from 0.59 to 0.84 mm diameter silica sand at a temperature of −12° C. Reduced ice contents help show the dependence of cohesion on the ice matrix and the dependence of the frictional component of strength on the sand material. Conclusions given below reflect the findings of this investigation.

1. The mechanical properties of frozen silica sand (initial void ratio of 0.59) in a confined stress condition are dependent on the cohesion of the ice matrix and the sliding friction, particle reorientation, and dilatancy effect of the sand grains. After the ice matrix fails at an axial strain close to one per cent, the sand resistance becomes a function of the normal stress. Development of frictional resistance may be reduced when sand pores are fully saturated with ice.

2. For confining pressures approaching 7 MN/m² and relatively dense sand samples, the cohesive component of strength appears to become very small.

3. Small changes in initial void ratio of the sand have a large influence on the stress–strain relationship of confined sand–ice materials.

4. Reduced ice contents appear to affect only the cohesion due to the ice matrix. For a constant temperature, the linear relation between degree of ice saturation and peak deviator stress suggests that decrease in strength is directly related to the area of ice in a cross-section of the sand–ice material.

5. Creep rates decrease exponentially and creep strength increases with an increase in confining pressure. Reduced ice contents appear to reduce the area of ice effective in the creep process without altering the basic creep process.

Acknowledgements

This study was supported by the National Science Foundation and the Division of Engineering Research, Michigan State University. Their support is gratefully acknowledged.

MS. received 7 February 1973

REFERENCES

Alkire, B. D. Unpublished. Mechanical properties of sand–ice materials. [Ph.D. thesis, Michigan State University, East Lansing, Michigan, 1972.]

Andersland, O. B., *and* AlNouri, I. 1970. Time dependent strength behavior of frozen soils. *Journal of the Soil Mechanics and Foundations Division, American Society of Civil Engineers*, Vol. 96, No. SM4, p. 1249–68.

Chamberlain, E., *and others*. 1972. The mechanical behaviour of frozen earth materials under high pressure triaxial test conditions, by E. Chamberlain, C. Groves and R. Perham. *Géotechnique* (London), Vol. 22, No. 3, p. 469–83.

Goughnour, R. R., *and* Andersland, O. B. 1968. Mechanical properties of a sand–ice system. *Journal of the Soil Mechanics and Foundations Division, American Society of Civil Engineers*, Vol. 94, No. SM4, p. 923–50.

Kaplar, C. W. 1971. Some strength properties of frozen soils and effect of loading rate. *U.S. Cold Regions Research and Engineering Laboratory. Special Report* 159.

Lambe, T. W., *and* Whitman, R. V. 1969. *Soil mechanics*. New York, John Wiley and Sons, Inc.

Lee, K. L., *and* Seed, H. B. 1967. Drained strength characteristics of sands. *Journal of the Soil Mechanics and Foundations Division, American Society of Civil Engineers*, Vol. 93, No. SM6, p. 117–41.

Schmertmann, J. H., *and* Osterberg, J. O. [1961.] An experimental study of the development of cohesion and friction with axial strain in saturated cohesive soils. (*In Research conference on shear strength of cohesive soils, sponsored by the Soil Mechanics and Foundations Division, ASCE, University of Colorado, Boulder, Colorado, June, 1960.* [New York], American Society of Civil Engineers, p. 643–94.)

Scott, F. S. 1969. The freezing process and mechanics of frozen ground. U.S. Cold Regions Research and Engineering Laboratory. *Cold regions science and engineering*. Hanover, N.H., Pt. II, Sect. D1.

Tsytovich, N. A., *ed.* 1959. *Osnovy geokriologii (merzlotovedeniya). Chast' pervaya. Obshchaya geokriologiya* [*Principles of geocryology (permafrost studies). Part one. General geocryology*]. Moscow, Izdatel'stvo Akademii Nauk SSSR. [English translation: "Chapter 5. Physical phenomena and processes in freezing, frozen and thawing soils". *Canada. National Research Council. Technical Translation* 1164, 1964.]

Vyalov, S. S. 1959. *Reologicheskiye svoystva i nesushchaya sposobnost' merzlykh gruntov* [*Rheological properties and bearing capacity of frozen ground*]. Moscow, Izdatel'stvo Akademii Nauk SSSR. [English translation: *U.S. Cold Regions Research and Engineering Laboratory. Translation* 74, 1965.]

Wu, T. H. 1966. *Soil mechanics.* Boston, Allyn and Bacon, Inc.